American Journal of Pathology, Vol. 153, No. 2, August 1998


# Animal Model

## Histopathological Characterization of Magnetic Resonance Imaging-Detectable Brain White Matter Lesions in a Primate Model of Multiple Sclerosis

### *A Correlative Study in the Experimental Autoimmune Encephalomyelitis Model in Common Marmosets* (Callithrix jacchus)

Bert A. 't Hart,* Jan Bauer,† Henk-Jan Muller,‡ Bert Melchers,§ Klaas Nicolay,‡ Herbert Brok,* Ronald E. Bontrop,* Hans Lassmann,† and Luca Massacesi¶

*From the Department of Immunobiology,* Biomedical Primate Research Centre, Rijswijk, The Netherlands; Institute of Neurology,† University of Vienna, Vienna, Austria; Bijvoet Centre and Image Sciences Institute,‡ Utrecht University, Utrecht, The Netherlands; TNO-PML, Pharmacology Research Group,§ Prins Maurits Laboratory, Rijswijk, The Netherlands; and Department of Neurological and Psychiatric Sciences,¶ University of Florence, Florence, Italy*

**Experimental autoimmune encephalomyelitis in the common marmoset, a nonhuman primate species (*Callithrix jacchus*), is a new model for multiple sclerosis. Given the close immunological relationship between marmosets and humans, it is an attractive model for investigating immunopathological pathways relevant to multiple sclerosis and to evaluate new treatments for the disease. Unlike in the originally documented model, experimental autoimmune encephalomyelitis induced without the use of *Bordetella pertussis* led to a chronic disease of moderate severity. The clinical course of experimental autoimmune encephalomyelitis in the present model was mainly chronic and progressive, but periods of incomplete remission did occur. At the chronic stage of the disease, actively demyelinating lesions were found together with inactive demyelinated and remyelinated (shadow) plaques. Before immunization and during clinically active experimental autoimmune encephalomyelitis, T1- and T2-weighted magnetic resonance brain images were obtained. Correlation of the data from the magnetic resonance images and the neuropathology analysis revealed that the hyperintense regions in T2-weighted images represented both active and inactive remyelinating lesions. Quantification showed that the number of lesions in T2-weighted magnetic resonance images equalled those found by pathological examination, and thus T2-weighted magnetic resonance imaging can be used to discern the total lesion load. Extravasation of gadolinium-diethylenetriamine-penta-acetic acid (triple dose) was found only in lesions, which by histopathology were shown to be engaged in the process of active demyelination. *(Am J Pathol 1998, 153:649–663)***

Multiple sclerosis (MS) is a chronic inflammatory and demyelinating disease of the central nervous system (CNS). Although there is a large variability among individual patients, MS typically follows a chronic-progressive or relapsing-remitting course. In the latter case, dis-

Supported by the European Union (EU) Human Capital and Mobility program (ERBCHGECT 940071, "Nonhuman Primates as Models for Human Biology and Disease"), by the EU Concerted Action on T-Cell Autoimmunity in Multiple Sclerosis, by the Dutch MS Foundation (Stichting Vrienden MS Research; grant 95-221MS), by an EU grant for the Scheikundig Onderloeu in Nederland-NMR Large-Scale Facility for Biomolecular NMR, and by the EU shared-cost project "CD40 Immunotherapy in Marmosets" (contract BMH4-CT.97-2131).

Accepted for publication May 2, 1998.

Address reprint requests to Dr. Bert A. 't Hart, Department of Immunobiology, Biomedical Primate Research Centre, PO Box 3306, 2280 GH Rijswijk, The Netherlands. E-mail: hart@bprc.nl.

Bert A. 't Hart and Jan Bauer contributed equally to this study.

ease episodes with neurological abnormalities (relapse/exacerbation) alternate with periods of partial or complete recovery (remission). The typical histopathological hallmark of MS is the presence of inflammatory, demyelinating lesions within the CNS. Most of these lesions contain mononuclear cells such as lymphocytes and macrophages, whereas granulocytes are not typically found. Demyelinated lesions are found throughout the CNS in a perivascular or periventricular location.[1]

Magnetic resonance imaging (MRI) is presently the diagnostic imaging modality of choice in MS.[2–4] T2-weighted sequences are especially sensitive to structural alterations of CNS tissue. All lesion stages, from early inflammation to late chronic stages, are visualized as hyperintense regions. Therefore, T2-weighted MRI is usually applied to assess the spatial distribution of plaques and to determine the total lesion load.[5] Active lesions can be distinguished from inactive ones by increased permeability of the blood-brain barrier (BBB) for intravenously injected gadolinium. This results in local enhancement of the signal intensity of T1-weighted images. Lesions with contrast-induced regional signal enhancement correlate well with disease activity both in MS[6–9] and in the experimental model experimental autoimmune encephalomyelitis (EAE).[10] However, limited information is available on pathological characteristics of MRI-detectable lesions.

The objectives of this study were to investigate the histopathological basis of MRI-detectable lesions in the EAE model in marmoset monkeys. The obvious advantage of any EAE model is that MR images can be recorded before and at defined time points after disease onset. When regions of interest appear in MRI, animals can be sacrificed immediately after *in vivo* MRI analysis to characterize regions of interest by immunohistopathological techniques. The EAE model in marmosets is of particular interest in view of the close similarity between the human and marmoset immune systems.[11–15]

The present study shows that the development of lesions in the marmoset brain white matter can be very well visualized with MRI techniques similar to those used for diagnosis of MS. Moreover, for histopathological characterization of MRI-detectable lesions, the same reagents could be used as those applied for the stage characterization of lesions in the CNS of MS patients. Our present pathological investigation reveals the presence of both active and inactive, as well as remyelinating, plaques in the CNS of EAE-affected marmosets that strongly resemble the plaques in the CNS of MS patients. Correlation of MRI and pathology revealed that the number of lesions in tissue sections equalled those found by T2-weighted MRI. Furthermore, none of the pathologically defined inactive lesions displayed gadolinium enhancement. Nearly all lesions that did show gadolinium enhancement of the T1-weighted nuclear magnetic resonance (NMR) signal could be classified as early active. In summary, we demonstrate here that the present EAE model resembles MS not only in its clinical expression, but also in radiological and histopathological aspects of the lesions that are found in the CNS white matter.

## Materials and Methods

### Monkeys

Eleven marmosets (*Callithrix jacchus*) were used for this study. The sex and birth dates (month/year) of the monkeys were: EB: male, 4/1992; EC: male, 8/1990; ED: female, 6/1992; EE: male, 4/1992; EG: female, 8/1992; EH: male, 6/1992; EI: male, 8/1992; EJ: male, 4/1993; EK: male, 4/1993; EL: male, 4/1993; and GY: male, 7/1994. The body weight of the monkeys at the start of the experiment ranged between 295 and 320 g. The monkeys were bred and raised at the Biomedical Primate Research Centre (Rijswijk, The Netherlands). Marmosets of either sex can be used, because there is no sex-linked difference in susceptibility to EAE. During the experiments, the monkeys were individually housed in spacious cages with padded shelter on the bottom. The daily diet consisted of commercial food pellets for nonhuman primates (Hope Farms, Woerden, The Netherlands), supplemented with rice and fresh fruit. Drinking water was provided *ad libitum*.

### EAE Induction

Myelin was isolated as described[16] from human brain white matter, which was kindly provided by Dr. Rivka Ravid of the Dutch Brain Bank (Amsterdam, The Netherlands). The myelin concentration in the stock solution was 30 mg/ml on a dry-weight basis and 1.3 mg/ml protein on a protein basis as measured according to Bradford.[17]

In a first group of five monkeys (EB, EC, ED, EE, and EG), EAE was induced essentially as described earlier.[18,19] The myelin stock solution was emulsified in an equal volume of enriched complete adjuvant. Enriched complete adjuvant was prepared by mixing incomplete adjuvant (DIFCO Laboratories, Detroit, MI) with 6 mg/ml desiccated mycobacteria (*Mycobacterium tuberculosis*, H37A, DIFCO) followed by brief sonication. Under ketamine anesthesia, each monkey was injected intradermally on the back with 600 $\mu$l of emulsion divided over four spots, two in the inguinal and two in the axillary region. In addition, 1 ml phosphate-buffered saline (pH 7.4) containing $10^{10}$ heat-inactivated *B. pertussis* particles was injected immediately after immunization and 48 hours later.

In a second group of six monkeys, the original immunization protocol was modified in two respects. First, the *Mycobacterium* concentration in the antigen-adjuvant emulsion was reduced from 1.5 to 0.5 mg/ml to diminish the severity of ulceration around the injection sites. Secondly, *B. pertussis* administration as second adjuvant was omitted to obtain a milder EAE in which patterns of EAE reactivity can be associated with the presence of certain mhc alleles and cytokine profiles.[20,21]

### Clinical Diagnosis

The clinical course of EAE was recorded daily by a trained observer using semiquantitative scoring: 0 = no

Table 1. Histopathology of EAE in Marmosets Induced With and Without Bordetella

| Animal | *Bordetella** | Time point† | Clinical score‡ | Inflammation§ | Infiltrate composition | DEM¶ | Lesion activity‖ | Brain lesion topography | Spinal cord** |
|---|---|---|---|---|---|---|---|---|---|
| EB | + | 21 | 3.0 | ++ | Ly, MΦ | ++ | A | Opt, Fo | +++ |
| EC | + | 13 | 3.0 | ++ | Ly, MΦ | + | A | CSO, Opt | ++ |
| ED | + | 6 | 3.0 | + | Ly, MΦ | +/− | A | CSO, CWM | + |
| EE | + | 13 | 3.0 | + | Ly, MΦ | − | I | CSO, Opt | − |
| EG | + | 11 | 4.0 | +++ | Gr, Ly, MΦ | ++ | A | CSO, Thal | +++ |
| EH | − | 76 | 1.0 | ++ | Ly, MΦ | ++ | A < I | Opt, CC, CI, CSO | ++ |
| EI | − | 35 | 2.0 | +++ | Ly, MΦ | +++ | A < I | Opt, CC, CI, CSO, Thal | ++ |
| EJ | − | 35 | 2.5 | +/− | Ly, MΦ | ++ | A < I | CC, Cer, Med Obl | + |
| EK | − | 24 | 2.5 | ++ | Ly, MΦ, Gr | ++ | I | CC, CSO | + |
| GY | − | 12 | 2.5 | +++ | Ly, MΦ | +++ | A > I | Opt, CC, CI, CSO, Thal | ++ |

Ly, lymphocytes; MΦ, macrophages; Gr, granulocytes; Opt, optic system; Fo, fornix; CSO, centrum semiovale (periventricular white matter); CWM, cerebellar white matter; Thal, thalamus; CC, corpus callosum; CI, capsula interna; Med Obl, medulla oblongata; Cer, cerebellum.

*+, with *Bordetella*; −, without *Bordetella*.

†Time point (weeks after immunization) at which each animal was sacrificed.

‡Clinical score at time of sacrifice.

§0, no inflammation; +, rare (1 to 3 perivascular cuffs/section); ++, moderate numbers (3 to 10) of perivascular cuffs/section; +++, widespread perivascular cuffing and parenchymal infiltration.

¶Demyelination: +/−, single demyelinated fibers; +, perivenous demyelination; ++, perivenous demyelination and some confluent plaques; +++, multiple confluent plaques.

‖A, active lesions; I, inactive lesions (<, less than; >, more than).

**−, no involvement; +, limited involvement; ++, moderate involvement; +++, extensive involvement.

clinical signs; 0.5 = apathy, loss of appetite, altered walking pattern without ataxia; 1 = lethargy and/or anorexia; 2 = ataxia; 2.5 = para- or monoparesis and/or sensory loss and/or brain stem syndrome; 3 = para- or hemiplegia; 4 = quadriplegia; 5 = spontaneous death attributable to EAE. The highest per-day scores were averaged over 1 week. Moreover, each monkey was weighed at least three times per week to obtain a more objective score of the clinical wellbeing.

### *MRI*

MRI was performed at the Bijvoet Center of Utrecht University, The Netherlands. For each monkey, T2- and T1-weighted magnetic resonance (MR) images were recorded, the latter also with contrast enhancement after intravenous injection of gadolinium-diethylenetriamine-penta-acetic acid (DTPA) (triple dose). The time points for performing MRI after immunization were chosen during periods of clinically active EAE.

### In Vivo *MRI*

In preparation for the experiment, the monkeys were anesthetized with ketamine/Vetranquil (9/1 v/v). During scanning, each monkey was placed on a 37°C water-filled heating pad (Granulab International BV, Amersfoort, The Netherlands) to prevent hypothermia. The head of the monkey was fixed in a custom-built stereotactic apparatus made of metal-free plastics to ensure reproducible positioning in the magnetic field and to minimize movement artifacts. The stereotactic apparatus was placed inside a saddle-type radiofrequency coil. MRI was performed on a SISCO 200-MHz spectrometer (Varian, Palo Alto, CA) equipped with an actively shielded gradient (maximum gradient 3.2 G/cm, 33 cm inner diameter).

### *Postmortem MRI*

T2-weighted MR images were recorded from formalin-fixed brains to enable the determination of the exact localization of the lesions that were detected *in vivo*. In both scannings the same orientation points were chosen for slice localization (see below). Because movement artifacts were absent and long acquisition times can be used, images of very high contrast can be obtained.

### *Slice Orientation and Scanning Procedure*

First, a sagittal scout scan was made. The posterior and anterior positions of the corpus callosum were chosen as orientation markers for precise localization of the slices for the *in vivo* and postmortem MRI. A T2 (echotime (TE)/repetition time (TR), 60/2500 ms)-weighted multislice scan (20 slices of 1 mm thickness) was obtained followed by a T1-weighted scan (TE/TR, 25/1000 ms) with the same spatial prescription. Gadolinium-DTPA (Magnevist; Schering AG, Berlin, Germany) was injected intravenously (0.3 mmol/kg) and allowed to circulate for 10 minutes to ensure adequate distribution. Next, the T1-weighted MRI was repeated to attain a postcontrast data set. Each slice was recorded with a matrix of 256 × 128 data points and a field of view of 5 × 5 cm. The data set was analyzed on an Apple Macintosh Performa 630 using the public domain NIH Image program.

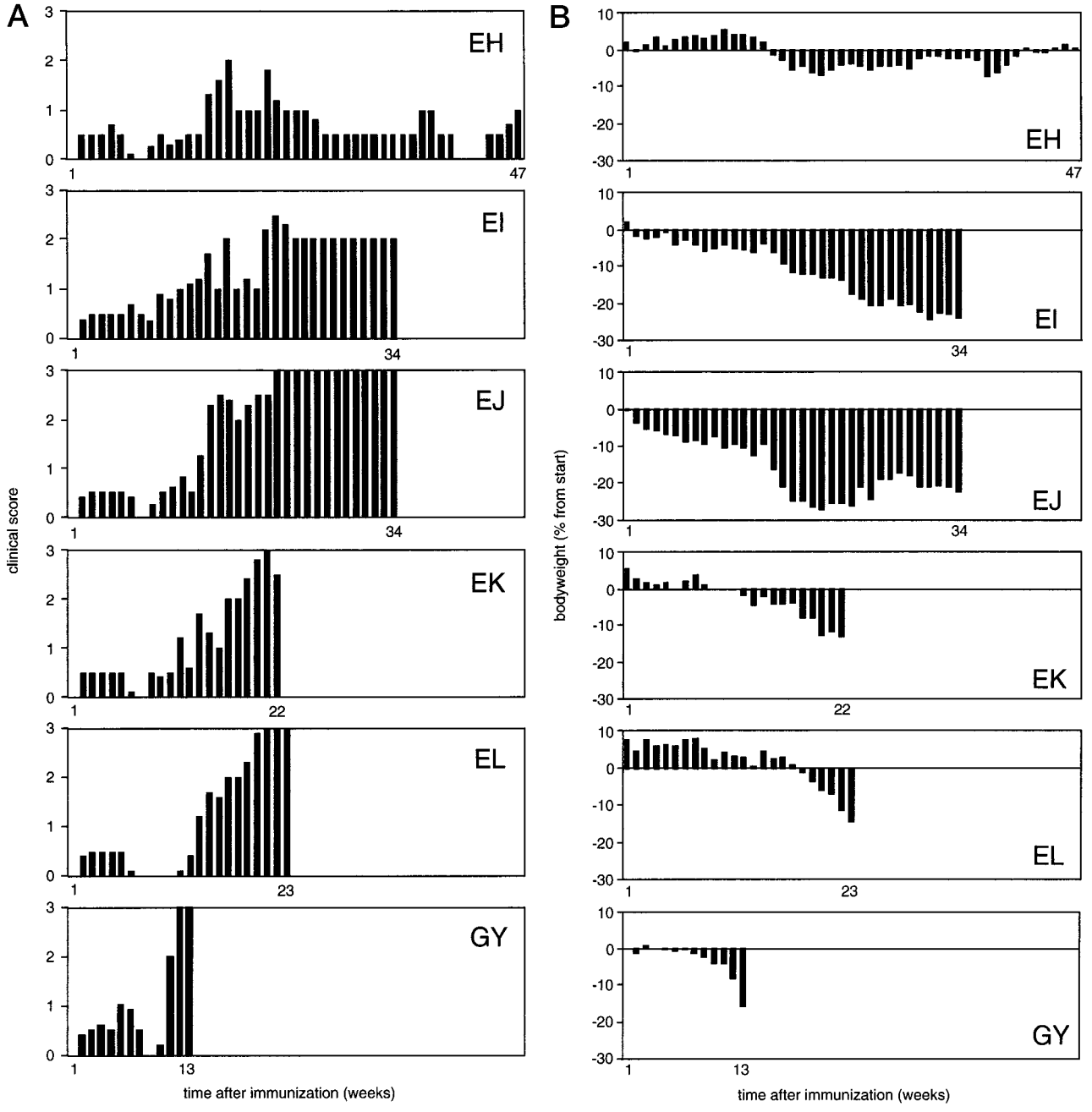


Figure 1. Course of EAE in marmosets. Six male marmosets were immunized with human myelin in complete adjuvant containing 1 mg/ml sonicated *Mycobacteria*. For each individual monkey, the mean clinical scores (see Materials and Methods) recorded in a week are given (A). The body weight, which serves as a surrogate disease marker, was measured at least twice weekly. For normalization, the body weights have been expressed as percentages of the measured weights at the start of the study (B).

Figure 2. MRI of monkey EI 34 weeks after induction of EAE. a and b: Two slices of postmortem T2-weighted MRI in the axial direction. Lesions are indicated with capitals in the figure. c and d: The corresponding slices in T2-weighted images, recorded 2 hours before sacrifice of the same monkey. e and f: The same slices in T1-weighted images, recorded 2 hours before sacrifice of the same monkey. Contrast enhancement by extravasation of gadolinium is apparent in two regions, I and C/D. In the *in vivo* T2-weighted images, ventricles and lesions are visible as the most hyperintense regions, whereas the most hypointense regions represent the white matter. The hyperintensity of lesion I (periventricular localization) seen in the T2 *in vivo* MRI (c) probably results from edema. Lesion I is much smaller in the postmortem MRI, probably because the formalin fixation changes the distribution of water in the parenchyma. Because of the absence of breathing artifacts and longer scanning times, postmortem images have a higher resolution in which lesions are visible as sharply demarcated hyperintense regions. As an example, in the postmortem T2 (d) and the T1 Gd-DTPA-enhanced MRI (f), a single hyperintense area (C/D) is present, which in the postmortem MRI (b) proves to be two separate lesions, of which one is located in the gray matter (C) and one in the white matter (D).

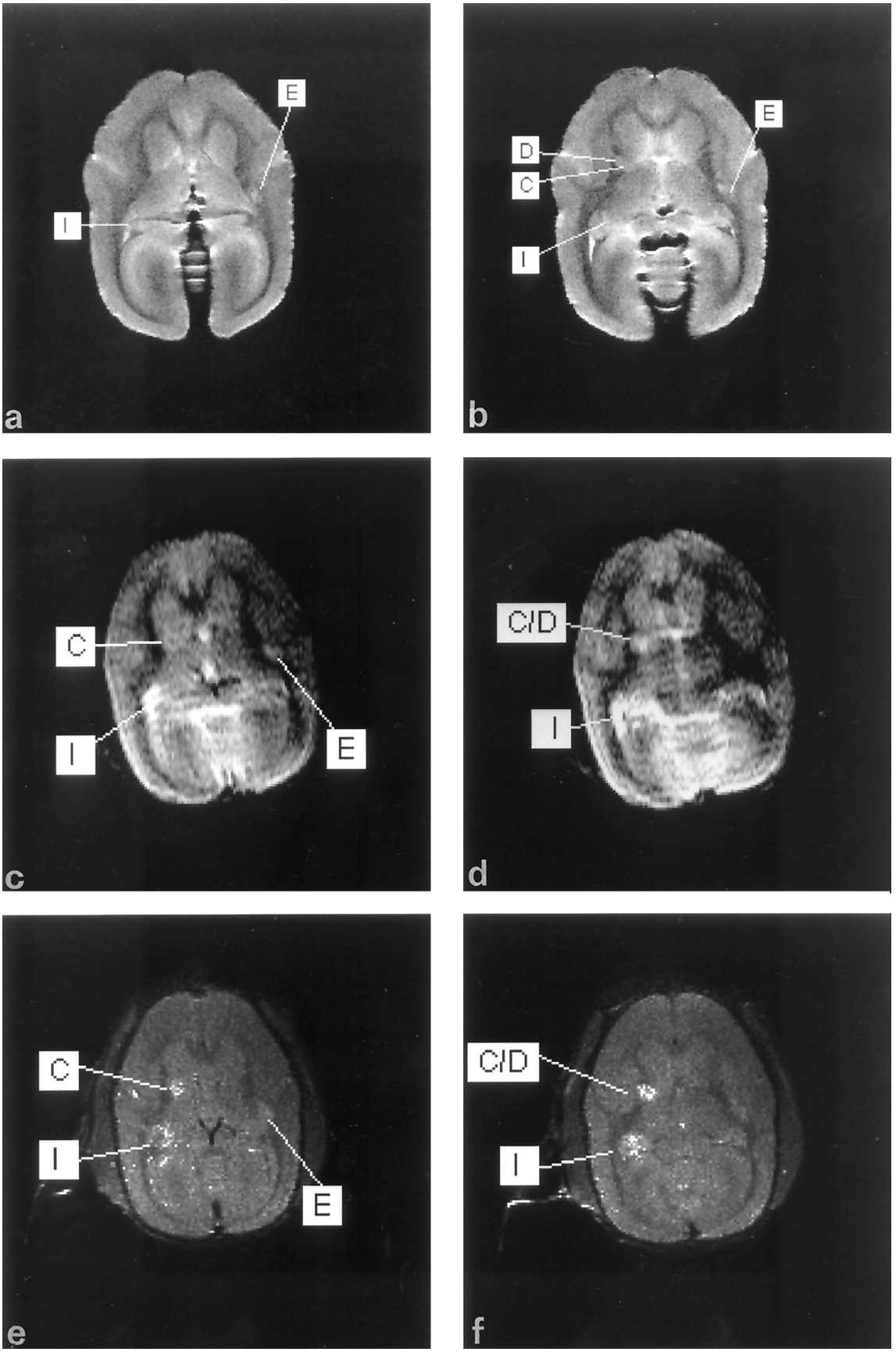
E
I
a
E
D
C
I
b
C
I
E
c
C/D
I
d
C
I
E
e
C/D
I
f

The T1-weighted MR images had an unexpected gray-white matter contrast. In images recorded with the NMR machines that are now used in clinical settings, which are 1.5 Tesla or less, a contrast conversion of the white and gray matter is normally seen on T1-weighted *versus* T2-weighted images. In T1-weighted images the NMR signal of the white matter is hyperintense in comparison with that of the gray matter, whereas in T2-weighted images the white matter signal is hypointense compared with that of the gray matter. In both the T1- and T2-weighted images recorded on our 4.7-Tesla machine, white matter is hypointense as compared with gray matter, and lesions are visible as hyperintensities. This is not a unique feature of the marmoset brain, given that it was also observed in cat brains (unpublished observation). The most likely explanation for this discrepancy is that with the high magnetic field used, T1 values of gray and white matter converge, whereas T2 values are unaffected by the strength of the field. In our T1-weighted images, the intensities of white and gray matter are most likely determined by the longer T2 value of gray matter and the different proton densities of both tissues. This phenomenon did not affect the detection of gadolinium enhancement, because even long TR/short TE images ("proton-density" weighted) contrast enhancement can be observed.[22]

### *Histopathology Analysis*

The brain and spinal cord of sacrificed monkeys were excised and fixed *in toto* for 3 days in 4% buffered formalin and subsequently stored at 4°C in phosphate-buffered saline, pH 7.4, containing sodium azide until analysis. In some experiments the fresh brain hemispheres were separated with a surgical blade, after which one hemisphere was fixed in buffered formalin and the other snap frozen in liquid nitrogen for immunohistological analysis. The analysis of the frozen brains has been published separately.[23] Formalin-fixed brains were embedded in paraffin. For the exact localization of lesions that were MRI detectable *in vivo*, use was made of the postmortem images. Because high-contrast images were made in the coronal and axial directions using the same orientation parameters as for the *in vivo* images, this enabled an accurate three-dimensional positioning of each lesion. From this material, coronal sections with a thickness of 3 to 5 $\mu$m were cut.

The extent of inflammation, demyelination, and axonal pathology was evaluated on tissue sections stained for hematoxylin and eosin to visualize infiltrated cells, with Klüver Barrera stain (Luxol Fast Blue (LFB) combined with periodic acid-Schiff (PAS)) for staining myelin and myelin degradation products and with Bielschowsky silver impregnation for staining axons. Immunocytochemistry was performed with a biotin-avidin system as described earlier.[24] T cells were stained with anti-human CD3 antibodies (Dakopatts, Glostrup, Denmark). Astrocytes were stained with polyclonal anti-glial fibrillary acidic protein (Dakopatts). Macrophages were detected by staining with the antibodies 27E10 and MRP14, which are both commercially available from BMA Biomedicals (Augst, Switzerland).[25] Myelin and oligodendrocytes were stained with antibodies recognizing 2′-3′-cyclic nucleotide-3′-phosphodiesterase (CNP; Affinity Research, Nottingham, UK), proteolipid protein (PLP) and myelin oligodendrocyte glycoprotein (MOG) which were kindly provided by Dr. S. Piddlesden (University of Cardiff, UK). Immunoglobulin (Ig) depositions in the lesions were detected using biotinylated anti-(human) Ig (Amersham, Buckinghamshire, UK) as a primary antibody. Depositions of complement factor C9 were detected by a polyclonal antibody as described earlier.[26]

### *Lesional Staging*

The maturation stage of a certain lesion was assessed using previously published criteria for the classification of MS lesions.[27] In this classification scheme, lesions are staged as follows: 1) early active lesions, presence of LFB and MOG myelin degradation products in macrophages and/or the presence of macrophages stained for macrophage antigen MRP14; 2) late active lesions, presence of myelin degradation products LFB and PLP but not MOG in macrophages and/or the presence of macrophages stained for macrophage antigens by 27E10 but not MRP14; 3) inactive lesions, presence of PAS-positive myelin degradation products but without LFB, PLP, or MOG degradation products in macrophages; and 4) remyelinated lesions, presence of thin LFB-positive myelin.

### *Ethics*

According to Dutch law on animal experimentation, the experimental procedures of this study have been reviewed and approved by the Institute's Animal Care and Use Committee.

## *Results*

In a first set of experiments, the originally documented EAE model in marmoset monkeys[18,19] was reproduced, namely by immunization with human myelin in complete adjuvant (with 3 mg *M. tuberculosis* per ml oil) and additionally intravenous administration of *B. pertussis*. As described in the original reports, this procedure induced a severe relapsing-remitting EAE. In our experience, however, the high *Mycobacterium* dose in the inoculum was found to cause large ulcerative skin lesions at the injection sites. This not only meant discomfort for the monkeys but also obscured early symptoms of neurological disorder in the lower part of the body. Furthermore, histopathological examination of CNS lesions showed that selective demyelination occurred only in small perivenous lesions. In the larger demyelinated lesions that were found around the ventricles, but only in one of the five monkeys (Table 1), the axons were completely disrupted, suggesting that the lesions were formed by a destructive inflammatory process rather than by selective demyelination. For these reasons we chose to further investigate EAE induced

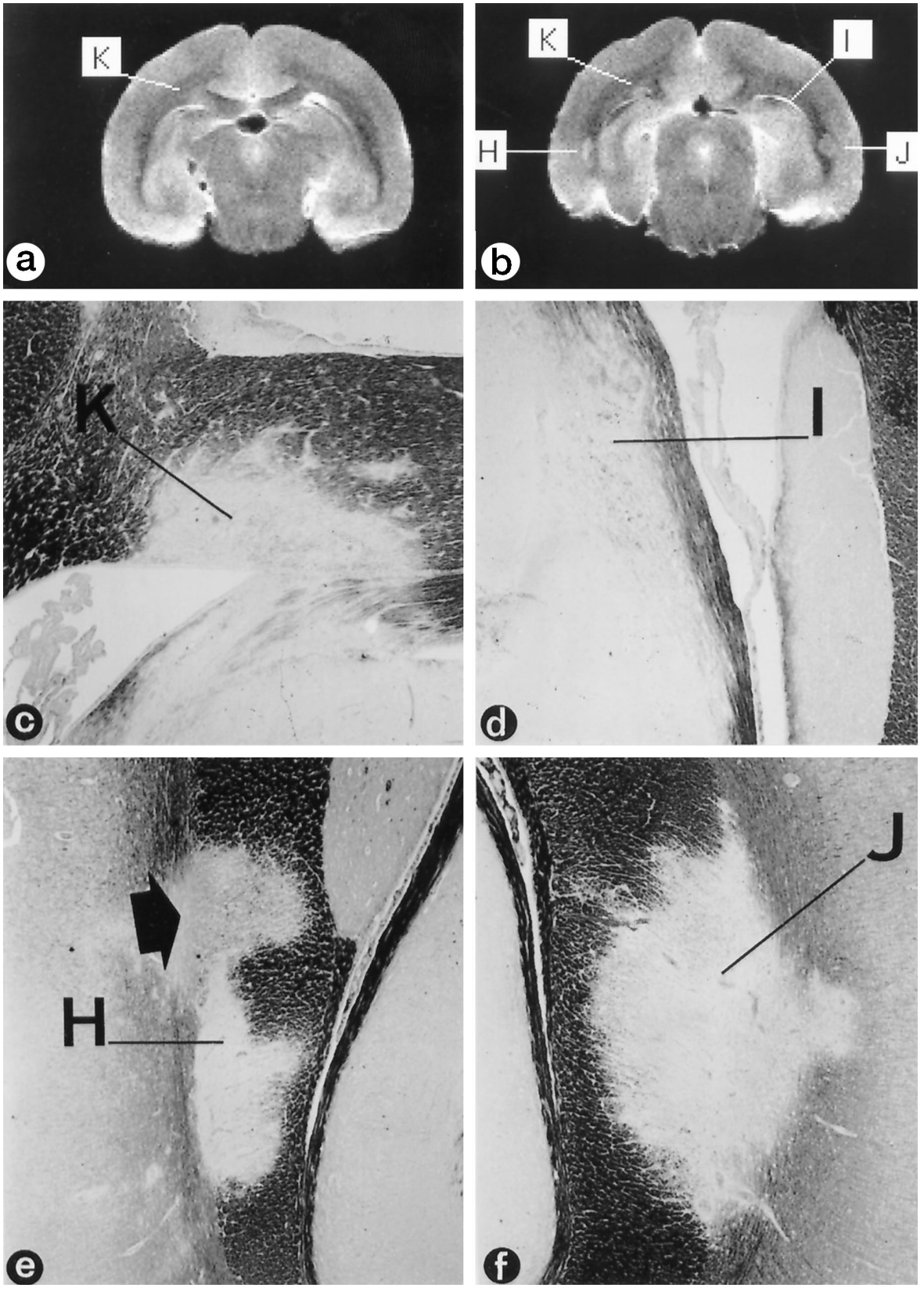


Figure 3. Correlation of T2-weighted MRI and histopathology. a and b: Two consecutive slices (coronal direction) of postmortem T2-weighted MRI of monkey EI. Klüver Barrera staining of the indicated regions H, K, I, and J are depicted in c to f (magnification, ×366), showing that these are demyelinated lesions. c: The periventricular lesion K, which is visible in both MR images, is an inactive demyelinated lesion showing signs of remyelination (see also Figure 5). d: Lesion I proved to be an early active periventricular lesion (see also Figure 4 and Table 5) showing strong gadolinium enhancement (see Figure 2, e and f). e: Region H is an inactive lesion in the corpus callosum, showing strong remyelination (arrow; see also Figure 5) in the upper part. The remyelinated and the nonremyelinated areas are visible in the T2-weighted MRI. f: Region J is a chronic lesion of which the upper part showed gadolinium enhancement (see also Table 5).

without administration of *B. pertussis* and using a reduced *Mycobacterium* dose in the inoculum.

## Clinical Expression of EAE

The clinical course of EAE was monitored using semiquantitative criteria (Figure 1a) and body weight measurement as a surrogate disease parameter (Figure 1b). All six monkeys developed a protracted form of EAE, but substantial interindividual variation of disease courses was observed. Monkey EH experienced several relatively mild attacks, maximally reaching score 2.0 (ataxia), with episodes of complete remission in between. This monkey went into remission in the 49th week and remained free of clinical signs up to week 76, when it was sacrificed for pathological examination. In the five other monkeys (EI, EJ, EK, EL, and GY), disease episodes of higher severity alternated with episodes of incomplete remission, as was particularly apparent from body weight measurements (Figure 1b). In the advanced stages of EAE, clinical remission in these monkeys was incomplete. Clinical signs progressed to paraparesis (EI) and hemiplegia (EJ) or paraplegia (EK, EL, and GY). Monkey EI was sacrificed after a long period of chronic ataxia, monkey EJ with one paralyzed leg and monkeys GY, EK, and EL with both legs paralyzed. Importantly, none of the monkeys in this experimental group died spontaneously.

## MRI Analysis of EAE

### In Vivo *MRI*

To visualize abnormalities in the brain white matter, T1- and T2-weighted MR data sets were recorded during episodes of active EAE. The first MR images were made of all monkeys in the 17th week after immunization. At that stage, regions with hyperintense signal intensity were found around the ventricles on T2-weighted images. Comparison with the T1-weighted images at that stage with those recorded before EAE induction, showed that the ventricles themselves were not enlarged. This observation points to periventricular edema (not shown). MRI recorded at later disease stages showed a number of circumscribed hyperintense regions within white matter tracts such as the corpus callosum, but also in cerebral gray matter (Figure 2, c and d).

### *Postmortem MRI*

To assess the total lesion load in the brain, a T2-weighted data set from all fixed brains was attained. These postmortem MR images were compared with the data from *in vivo* MR images, which were recorded 1 hour before the monkey was sacrificed. Because of the absence of movement artifacts, the postmortem images showed very high quality and contrast (Figure 2, a and b). As reported previously, the contrast in T2-weighted MR images of brain tissue before and after 6 weeks of fixation in buffered formalin is comparable.[28,29] In accordance with this, all hyperintensities that were detectable *in vivo* (Figure 2, c and d), were found in the postmortem images (Figure 2, a and b). Using the combined data from MR images made in the coronal (Figure 3, a and b) and axial (Figure 2, a and b) directions, the exact localization of each individual lesion in the fixed brain could be determined.

## Histopathology

Pathological investigation of animals with EAE induced without usage of *Bordetella* revealed the presence of inflammatory lesions with predilection sites in the cerebral white matter and spinal cord (Table 1). Except for some perivascular lesions, the cerebellum and medulla oblongata in these animals were practically devoid of inflammation. The cerebral lesions contained lymphocytes and macrophages, whereas accompanying granulocytes were sparsely found in some infiltrates in the brain of animal EK. In general, the demyelination in these animals led to the formation of large confluent plaques, which were visualized by Klüver Barrera stain (Figure 3, c to f) or immunocytochemical staining for the myelin proteins PLP (Figures 4e and 5a), CNP, and MOG. The CNS of animals EH, EJ, and EK also contained, in addition to the plaques, a large number of small demyelinated perivascular lesions. Staining by Bielschowsky impregnation revealed axonal reduction in active demyelinating plaques which, because almost no spheroids were present, occurred because of edema and the infiltration of large numbers of inflammatory cells (Figures 4h and 5e). In most older inactive plaques, axons were very well preserved. In a small minority of plaques, however, a highly reduced axonal density was seen (Table 2).

Based on the presence of inflammatory T cells (Figure 4c) and LFB- and PAS-positive degradation products in phagocytic macrophages, as well as on astrocytic scar formation, we concluded that in all animals, active as well as inactive lesions were present (Tables 1 and 2). In addition to the standard histopathology, a fine characterization of each lesion was made by analyzing the presence of certain macrophage subpopulations by staining

Figure 4. Immunopathology of active lesions in monkey EI. a: Staining of regions I and J for macrophage marker 27E10 (magnification, ×34). Note that lesion I (see also Figures 2 and 3) shows 27E10 reactivity close to the lateral ventricle but also deeper in the parenchyma. b: Higher-magnification (×335) 27E10-positive macrophages in lesion J. c: Staining of CD3+ve cells in lesion I, indicating strong T-cell infiltration (magnification, ×335). d: MRP-14-positive macrophages in lesion I (magnification, ×990). e: Staining of lesion J with *in situ* hybridization for PLP mRNA combined with immunocytochemistry for PLP. The edge of this lesion shows the presence of macrophages containing PLP degradation products (arrowheads). Outside the lesion, in between the myelin (red), PLP mRNA-positive oligodendrocytes (brown; arrows) are found. In the lesion itself some weakly stained remaining oligodendrocytes (arrows) are present (magnification, ×388). f: PLP staining of lesion I showing the presence of macrophages with PLP degradation products (magnification, ×684). g: The presence of MOG degradation products in macrophages in lesion I (magnification, ×792). h: Bielschowsky silver impregnation for axons showing the edge of lesion J. Inside the lesion, likely because of edema, the density of axons is lower as in the surrounding tissue (magnification, ×161). Active demyelination in lesion I might occur through an antibody- and complement-mediated mechanism. i: Deposition of Igs on bundles of myelin (arrow). The punctate staining indicates that these myelin sheaths undergo degradation (magnification, ×308). j: The staining for complement C9 reveals that the same bundles that are opsonized with Igs also show deposition of C9 (magnification, ×308).

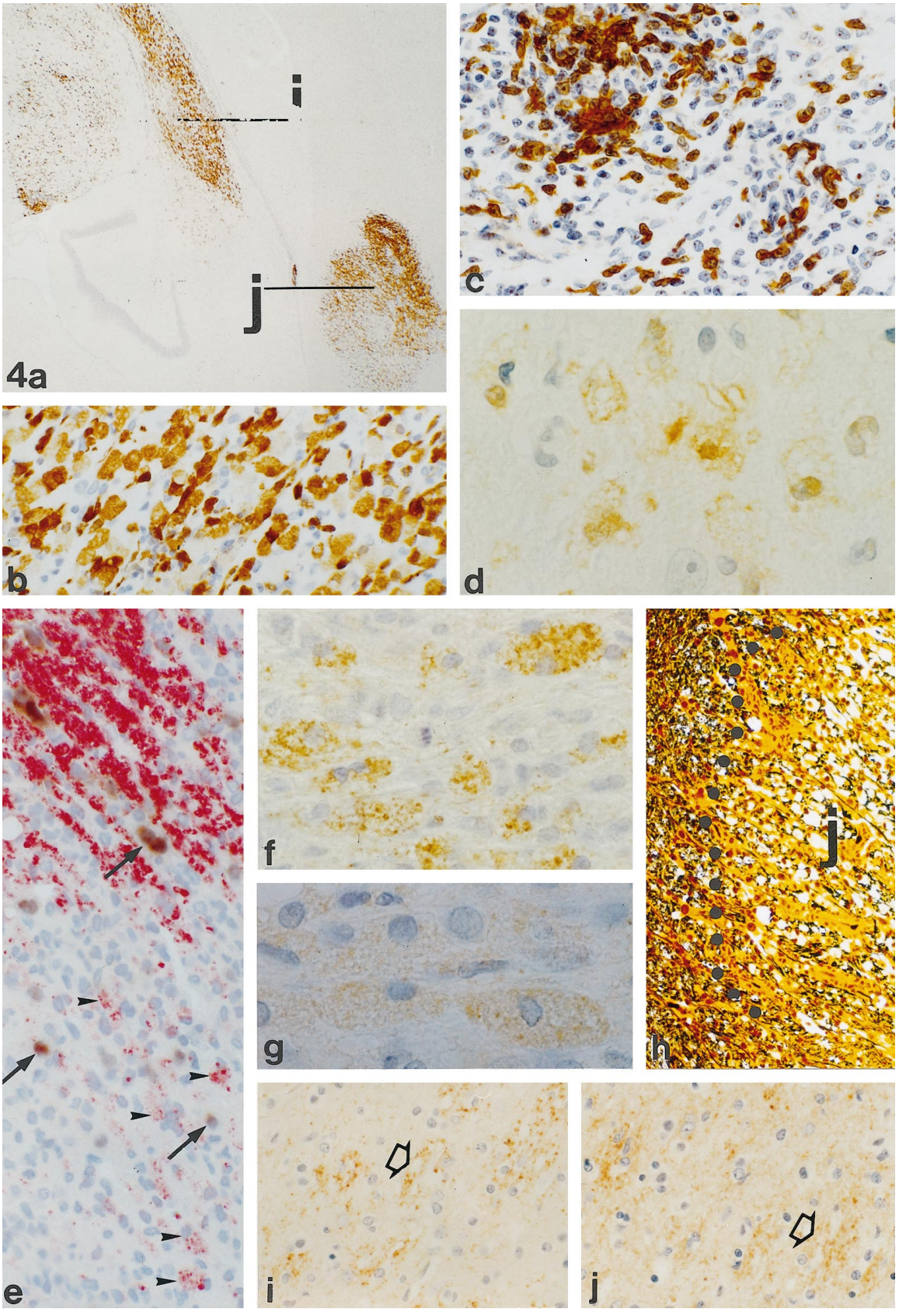
i
j
4a
c
b
d
e
f
g
h
j
i
j

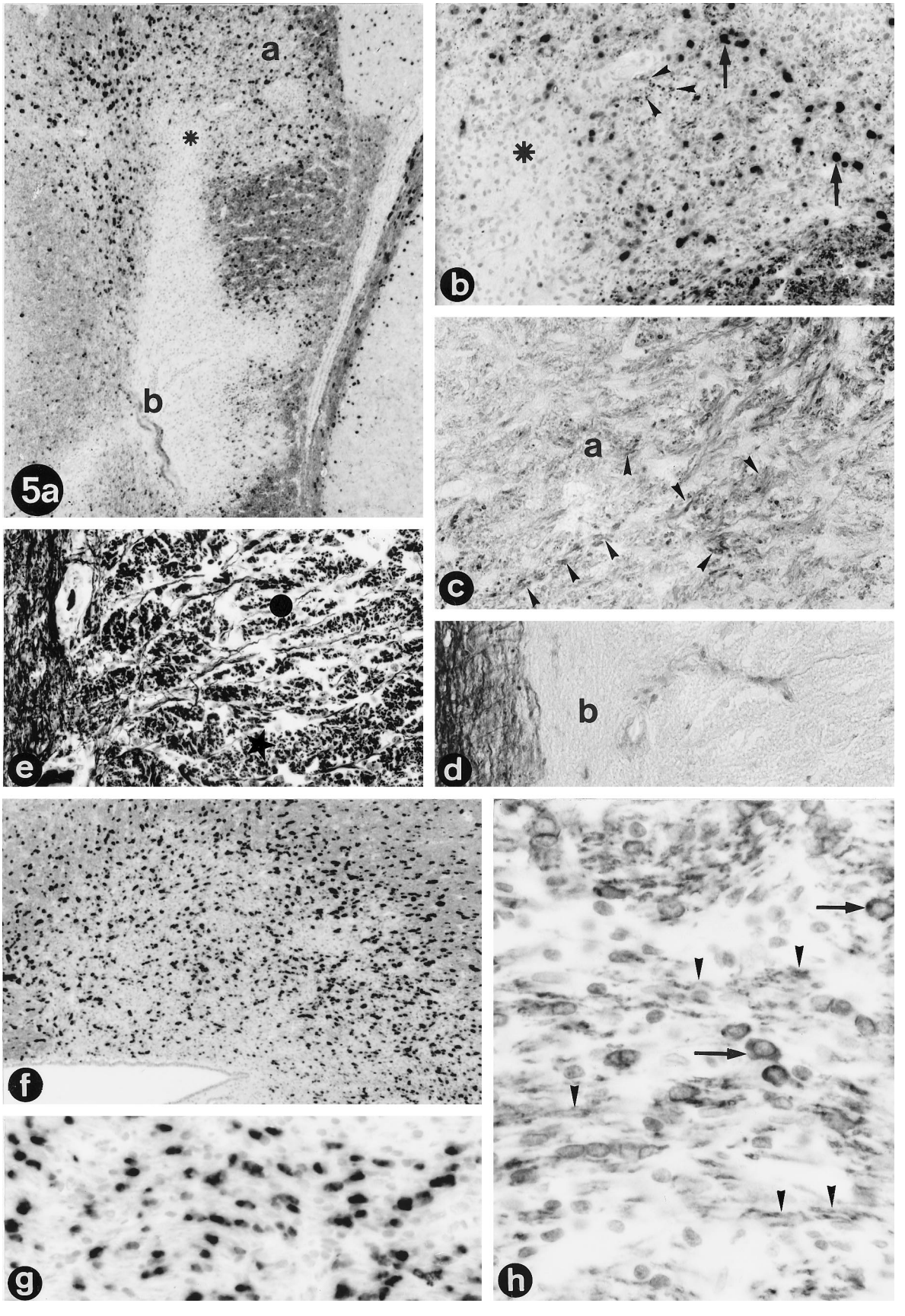
a
b
5a
b
c
a
e
d
b
f
g
h

Table 2. Characteristics of Active and Inactive Demyelinated Lesions

| Type of lesion | T cells | B cells | MΦ | Myelin breakdown | | Astrocytes/ gliosis | Axonal density |
|---|---|---|---|---|---|---|---|
| | | | | LFB | PAS | | |
| EA | + | +/− | + | + | − | Prot astr | Reduced* |
| LA | + | +/− | + | + | + | Fibr gliosis | Reduced* |
| IN | v | +/− | v | − | v | Fibr gliosis | Normal† |

MΦ, macrophages; EA, early active; LA, late active; IN, inactive; +, high number of cells; +/−, some cells; −, no cells; v, variable numbers of cells in different lesions; prot astr, protoplasmic (activated) astrocytes; fibr, fibrillary.
*Lower axonal density due to edema and infiltration of inflammatory cells rather than destruction of axons.
†Most lesions showed little/no axonal loss; a small number of lesions showed axonal loss.

with the antibodies 27E10 and MRP14 and for intracellular presence of MOG and PLP protein degradation products. Inactive demyelinated lesions, showing absence of LFB-positive material (Figure 5d) and only a moderate amount of PAS-positive myelin breakdown products in macrophages, also lacked staining with the macrophage markers 27E10 and MRP14. The macrophages in these lesions did not contain detectable amounts of MOG and PLP. In contrast, active lesions contained many macrophages that stained positively with the antibody 27E10 (Figure 4, a and b) and contained LFB-positive material. Macrophages expressing MRP14 (Figure 4d) and containing the myelin degradation product MOG (Figure 4g) were found only in some of the active lesions. The MOG and PLP staining showed that all KLB- and 27E10-positive lesions contained macrophages with intracellular inclusions of PLP-positive degradation products (Figure 4f).

Because Ig- and complement-mediated mechanisms are involved in myelin degradation in rodent EAE models, and possibly also in MS,[25,30] we have investigated the presence of Ig and complement factor C9 in demyelinated lesions. Ig deposition was found in a variety of lesions ranging from inactive to active. In some of the early active lesions, such as lesions D and I of animal EI, punctate Ig deposition was found on myelin sheaths, pointing to active myelin destruction (Figure 4i). Although Ig molecules were present in both active and inactive lesions, complement factor C9 could only be demonstrated in the (early active) lesions in a similar distribution as that of the punctate Ig deposition described above (Figure 4j).

Besides active and inactive demyelinated lesions, remyelinated plaques were also found (Figure 5). Remyelinated lesions, or shadow plaques due to the presence of very thin LFB-positive myelin sheaths (Figure 3e and 5c), showed strong staining of myelin and oligodendrocytes by immunocytochemistry for CNP (Figure 5h). Remyelinating activity was found not only in inactive lesions, but also in early and late actively demyelinating lesions. *In situ* hybridization for PLP mRNA revealed that areas of active remyelination contained high numbers of oligodendrocytes that expressed PLP mRNA in their cytoplasm (Figure 5, a, b, f, and g).

## *MRI-Pathology Correlation*

High-contrast T2-weighted MR images of fixed brains were recorded using the same parameters for slice orientation as used for *in vivo* MRI. The postmortem images were used to study the possible MRI-pathology correlation of lesions.

In animals EI and GY, virtually all confluent lesions that could be detected by histopathology were also visible in the postmortem T2-weighted MRI. However, no clearly diverse T2 signal intensities could be detected between lesions with different histopathological aspects (Figure 3 and Table 3). We are currently planning quantitative T2 measurements to investigate this issue in more detail. In animals EH, EJ, and EK, the correlation between pathology and MRI was more difficult. Many of the very small perivascular or periventricular lesions could not be retrieved in the corresponding MRI. Moreover, the majority of the small hyperintense regions in the T2-weighted MR images, eg, those in the corpus callosum of animal EK, were not found at the same place by pathological investigation. However, the total number of lesions that were found with pathology and MRI in the corresponding areas was similar (Table 4). This suggests that the discrepancy in correlation of pathology and MRI has a technical reason, such as small differences in the plane of sectioning, rather than that these lesions differ in T2 characteristics from larger "pathological" lesions that could be traced easily in MRI. Little is known on the MRI appearance of remyelinated lesions. Our present data show that, as predicted by Barkhof,[31] the shadow plaque K (Figures 3c

Figure 5. Remyelination and inactive lesions. **a**: Remyelination in lesion H of monkey EI (compare Figure 3, b and e), shown by *in situ* hybridization for PLP mRNA combined with immunocytochemistry for PLP. Small black dots indicate PLP mRNA-positive oligodendrocytes. Whereas the lower side of the lesion (indicated by b) shows the absence of oligodendrocytes and myelin, the upper side (indicated by a) shows high numbers of oligodendrocytes, indicating active remyelination. **b**: Higher magnification (×61) of the remyelination in the upper part of lesion H (compare position of asterisk in **a** and **b**). **Arrows** point at PLP mRNA-positive oligodendrocytes that are present in high numbers in the remyelinating area. The small dots (**arrowheads**) in between the oligodendrocytes are newly formed myelin sheaths staining positively for PLP protein (magnification, ×190). **c** and **d**: Klüver Barrera stain for myelin of lesion H. In **c**, the remyelinating part of lesion H is shown (the letter "a" in the figure corresponds with area "a" in part **a**). **Arrowheads** indicate newly formed LFB-positive fibers in this area (magnification, ×300). In **d**, the lower part of lesion H is depicted, corresponding with area b in part **a**. Unlike in the upper part, no LFB-positive fibers are present, indicating the lack of remyelination in this inactive lesion (magnification, ×300). **f**: *In situ* hybridization for PLP mRNA combined with immunocytochemistry for PLP protein of lesion K (see also Figure 3, a to c). Black dots indicate high numbers of PLP mRNA-positive oligodendrocytes in this remyelinating lesion (magnification, ×61). **g**: Higher magnification of lesion K showing the PLP mRNA-positive oligodedrocytes (magnification, ×238). **h**: Immunocytochemical staining for CNP shows strong staining of myelin fibers (**arrowheads**) and oligodendrocytes (**arrows**) in lesion K (magnification, ×350).

Table 3. Gadolinium Extravasation and Albumin Leakage in Early and Late Active Demyelinated Lesions in Monkeys EI and GY

| Lesion* | Gd-DTPA | Albumin | KLB | PLP | MOG | 27E10 | MRP14 | Lesion activity |
|---|---|---|---|---|---|---|---|---|
| Gadolinium-enhancing lesions | | | | | | | | |
| E1(GY) | + | + | + | + | + | + | ND | EA |
| E2(GY) | +/− | + | + | + | + | ++ | ND | EA |
| G(GY) | +/− | + | + | + | + | + | ND | EA |
| J(GY) | + | + | + | + | ++ | ++ | ND | EA |
| P(GY) | + | + | + | + | + | + | ND | EA |
| O(GY) | +/− | + | + | + | ND | + | ND | EA |
| C(EI) | + | + | + | ++ | + | ++ | ++ | EA |
| D(EI) | + | + | + | + | + | ++ | + | EA |
| I(EI) | + | + | + | ++ | + | ++ | + | EA |
| J(EI) | +/− | + | + | + | +/− | ++ | +/− | EA/LA |
| Lesions associated with gadolinium-enhancing lesions | | | | | | | | |
| H(GY) | − | + | + | + | + | ++ | ND | EA |
| I(GY) | − | + | + | + | + | + | ND | EA |
| M(GY) | − | + | + | + | + | + | ND | EA |
| N(GY) | − | + | + | + | + | ++ | ND | EA |
| Lesions not associated with gadolinium-enhancing lesions | | | | | | | | |
| K(GY) | − | + | + | + | ND | ++ | ND | EA/LA |
| L(GY) | − | + | + | + | ND | + | ND | LA |
| F1(GY) | − | ND | + | + | +/− | +/− | ND | LA |
| F2(GY) | − | ND | + | + | +/− | +/− | ND | LA |
| Q(GY) | − | + | + | + | − | + | ND | LA |

*Lesion: name of lesion; the name of the monkey is given in parentheses. −, no reactivity; +/−, some reactivity or reactivity in part of the lesion; +, reactivity throughout the lesions; ++, strong reactivity/high numbers of immunoreactive cells. EA, early active lesion; LA, late active lesion; ND, not done.

and 5f) appears as a hyperintense region in T2-weighted MRI (Figure 3a).

Of particular interest is the correlation between the activity characterization of a given lesion based on histopathological and MRI criteria. Ten out of 14 lesions that showed early demyelinating activity, ie, MOG-positive myelin breakdown products in macrophages and/or presence of MRP14-positive macrophages, displayed gadolinium enhancement (Table 3). A false negative score may occur when the amount of extravasated gadolinium is too low to cause a detectable change of the T1-weighted NMR signal intensity (partial volume effect). This may take place when extravasation occurs only in peripheral parts of a lesion. Hence, lesions that were peripheral parts of a gadolinium-enhancing lesion were analyzed as a separate group within the pathologically defined demyelinating lesions (Table 3). With this precaution in mind, all gadolinium-positive lesions could be classified as early demyelinating lesions, containing high numbers of MOG-positive macrophages (Tables 3 and 5). Gadolinium-negative lesions that are closely associated with gadolinium-positive lesions were shown to be early active lesions too. However, gadolinium-negative lesions that were not associated with gadolinium-positive lesions contained PLP-positive or 27E10-positive macrophages, but MOG- or MRP14-positive macrophages were absent, and these were, therefore, classified as late active (Tables 3 and 5). None of the pathologically defined inactive lesions ($n = 58$) displayed gadolinium enhancement of the T1-weighted NMR signal intensity (Table 5).

Gadolinium enhancement of T1-weighted images detects extravasation of the paramagnetic molecules through a disrupted BBB. As a confirmatory histological marker for BBB leakage, the MRI-detectable lesions were stained for the presence of albumin. Strong albumin immunoreactivity was found both in gadolinium-enhancing as well as gadolinium-nonenhancing early and late demyelinating lesions, suggesting that in the nonenhancing lesions, BBB leakage may have taken place before the

Table 4. Comparison of the Numbers of Lesions Detected with Pathology and MRI

| Animal | Total lesions in pathology | Total lesions in T2MRI | Dem. lesions in pathology* | DEM/REM activity | | | |
|---|---|---|---|---|---|---|---|
| | | | | EA | LA | IN | REM |
| EI | 18 | 20 | 13 (12) | 4 | 0 | 9 | 7 |
| EH | 56† | 65 | 22‡ (4) | 0 | 3 | 19 | 4 |
| EJ | 31† | 38 | 17‡ (8) | 0 | 2 | 15 | 3 |
| EK | 40†§ | 35 | 10 (6) | 0 | 0 | 10 | 3 |
| GY | 25 | 26 | 20 (16) | 11 | 4 | 5 | 5 |

EA, early active; LA, late active; IN, inactive; REM, remyelinating; DEM, demyelinating.
*Demyelinated lesions; numbers in parentheses indicate numbers of demyelinated lesions that are detectable in T2 MRI and of which a corresponding lesion in pathology was found.
†Contained many small perivascular lesions.
‡Contained a number of small lesions with perivascular demyelination.
§Contained a number of shadow plaques, which were not further characterized with histopathology.

Table 5. T1 and T2 Characteristics of the Different Types of Lesions

| Lesion | MRI characteristics | | |
|---|---|---|---|
| | T2 (postmortem) | T1 | T1-Gd-DTPA |
| Early active | Hyperintense | Hyperintense > isointense | Enhancing |
| Late active | Hyperintense | Isointense > hyperintense | Nonenhancing |
| Inactive | Hyperintense | Isointense > hyperintense | Nonenhancing |
| Remyelinating | Hyperintense | Isointense > hyperintense | Nonenhancing |

MR images were made. In (nonenhancing) inactive lesions, only weak albumin immunoreactivity was found (data not shown).

## *Discussion*

The aim of this study was to analyze histopathological characteristics of MRI-detectable lesions and to evaluate sensitivity and specificity of the most commonly used MRI acquisitions in a valid animal model of MS. For this purpose, chronic EAE was induced in a panel of randomly selected marmosets. At different time points during the course of EAE, MR images were made, after which animals were sacrificed for histopathological examination.

The current histopathological characterization of demyelinating activity in lesions is based on the presence of material positive for LFB, PAS, or Oil Red O (for neutral lipids) in phagocytic macrophages. However, especially PAS and Oil Red O positivity in macrophages can be found for more than 6 months after a new demyelinating lesion has developed, which implies that the presence of PAS- and Oil Red O-positive material may not always reflect ongoing demyelination.[25] Recent studies have shown that the presence of myelin protein breakdown products, such as MOG, myelin basic protein, or PLP, in macrophages gives a more accurate characterization of the stage of demyelinating lesions.[27,32] Early stages of demyelination can also be distinguished by the expression of the macrophage activation markers MRP14 or 27E10.[27] By combination of the classical and the new markers, a stringent stage characterization of demyelinating lesions can be made. By using these criteria for lesional staging, we were able to demonstrate that essentially all types of lesions present in MS brain (perivascular, paraventricular, active, and inactive demyelinating and remyelinating) are also present in EAE-affected marmoset brains. We conclude therefore that in the present model the main characteristics of MS pathology can be found. The fact that the same set of markers can be used for the pathological characterization of the lesions in the CNS of MS patients as in the marmoset model is of great value for extrapolation of experimental and patient data.

This report documents the correlation of radiological (MRI) and histopathological characteristics of the CNS white matter lesions in the marmoset EAE model. Normal brain tissue is highly organized, determining the typical MR relaxation times. The standard T2-weighted sequences are very sensitive to structure disturbances representing all stages of lesion formation as hyperintense regions. Therefore, in human brain, T2-weighted MR images are very suitable for assessing the spatial lesion distribution, but because of the inherent low specificity the images provide only little information on the nature of lesions.[29] Our data show that the shape and localization of the MRI-detectable lesions in the brain of marmosets developing EAE resembles the situation in the CNS of MS patients. In accordance with data from others, the T2-weighted MR images made of formalin-fixed brains do not essentially differ from the T2-weighted images made *in vivo*.[28,31] We have used high-contrast postmortem MRI for exact three-dimensional localization of lesions of interest for further characterization with histology. In the pathology and MRI analysis of marmoset brains, similar numbers of lesions were counted, indicating that, as in humans, T2-weighted MRI can be used to determine the total lesion load.

Extravasation of intravenously injected gadolinium is a radiological criterion for active lesions that can be seen as focal enhancement of T1-weighted signal intensity. By using a whole set of histopathological parameters, we were able to demonstrate 1) that all early active lesions display gadolinium enhancement in T1-weighted MRI and 2) that, with the exception of one lesion (K), all nonenhancing lesions could be characterized as inactive or late active lesions. A discrepancy exists in a subgroup of pathologically defined active lesions, which are located very close to gadolinium-enhancing lesions in adjacent scans, but which displayed no detectable extravasation of gadolinium. The discrepancy between the histological and radiological markers for BBB leakage may have a technical reason, ie, that gadolinium extravasation in only a small part of a lesion may yield an insufficient concentration of the paramagnetic molecule to exert a visible effect on the T1-weighted NMR signal intensity of the whole lesion (partial volume effect). Another explanation for the detection of albumin and the absence of gadolinium is that leakage of molecules such as albumin and Igs from serum to the brain is a continuous phenomenon, whereas gadolinium-DTPA is given in a single injection and therefore may reach concentrations too low to detect in the late active lesions.

As indicated in Table 5, many lesions appear as hyperintensities in our *in vivo* T1-weighted images. Given the virtual lack of axon pathology, structures such as "black holes" could not be expected. Moreover, no apparent correlation with certain stages of lesion differentiation could be found. We have no explanation for the observed phenomenon, and comparable to the different T1 values of gray and white matter (see Slice Orientation and Scanning Procedure, in Materials and Methods), we

like to attribute it to the high magnetic field. Experiments are now in preparation to quantitate NMR signal intensities of individual lesions to correlate these data with quantitative immunohistochemical criteria of demyelination, remyelination, and axonal loss. We are also investigating whether administration of a higher Gadolinium dosage than the currently used triple dose may increase the numbers of detectable lesions with BBB leakage or demyelinating activity.

In summary, the new marmoset EAE model is a valid experimental model for human MS in which lesion formation can be investigated with MRI and pathology. In view of the central role of autoimmune factors in the etiopathogenesis of MS, the high similarity of the human and marmoset immune systems is of great importance. In this respect, a high degree of homology in the genes encoding for T-cell receptor subunits[15] and major histocompatibility complex molecules (Ref. 16 and S.G. Antunes et al, submitted), as well as significant immunological cross-reactivity of lymphocyte surface markers and cytokines, have been documented.[11–13,23] These collective data make this model a unique tool for basic research in MS and EAE and for preclinical evaluation of new therapies for MS.

## Acknowledgments

The authors acknowledge B. Groen, A. Arkesteijn, and Dr. I. Philippens for expert care of the marmosets; C. de Groot, H. Koning, H. Breitschopf, E. Gurnhofer, M. Leisser, and A. Kury for technical assistance; Dr. P. van Eerd for veterinary care; Drs. E. Kuhn and S. Klumpp for the necropsies; and G. van Vliet for building the stereotactic apparatus. We thank Prof. Dr. Paul van der Valk and Dr. Frederik Barkhof (Free University, Amsterdam, The Netherlands) for critical review of the manuscript and H. van Westbroek for the artwork.

## References

1. Adams CWM: The general pathology of multiple sclerosis: morphological and chemical aspects of the lesions. Multiple Sclerosis: Diagnosis and Management. Edited by JF Hallpike, CWM Adams, WW Toutelotte. London, Chapman and Hall, 1983
2. Thorpe JW, Miller DH. MRI: its implication and impact. Int Mult Scler J 1994, 1:7–15
3. Young IR, Hall AS, Pallis CA: Nuclear magnetic resonance imaging of the brain in multiple sclerosis. Lancet 1981, 2:1063–1066
4. McFarland HF: Clinical trials in multiple sclerosis. Controlled Clinical Trials in Neurological Disease. Edited by RJ Porter, BS Schoenberg. Boston, Kluwer Academic, 1990, pp 321–341
5. Harris JO, Frank JA, Patronas NJ, McFarlin DE, McFarland HF: Serial Gd-enhanced magnetic resonance imaging scans in patients with early, relapsing-remitting multiple sclerosis: implications for clinical trials and natural history. Ann Neurol 1991, 29:548–555
6. Thompson AJ, Kermode AG, Wicks D, MacManus DG, Kendall BE, Kingsley DPE, McDonald WI: Major differences in the dynamics of primary and secondary progressive multiple sclerosis. Ann Neurol 1991, 29:53–62
7. Barkhof F, Scheltens P, Frequin STFM, Nauta JJP, Tas MW, Valk J, Hommes OR: Relapsing-remitting multiple sclerosis: sequential enhanced MR imaging vs. clinical findings in determining disease activity. Am J Roentgenol 1992, 159:1041–1047
8. Van Walderveen MAA, Barkhof F, Hommes OR, Polman CH, Tobi H, Frequin STFM, Valk J: Correlating MRI, and clinical disease activity in multiple sclerosis: relevance of hypointense lesions on short-TR/short TE (T1-weighed) spin-echo images. Neurology 1995, 45:1684–1690
9. Hawkins CP, Munro PMG, MacKenzie F, Kesselring J, Tofts PS, du Boulay EPGH, Landon DN, McDonald WI: Duration and selectivity of blood-brain-barrier breakdown in chronic relapsing experimental allergic encephalomyelitis studied by Gd-DTPA and protein markers. Brain 1990, 13:365–378
10. Morrissey SP, Stodal H, Zettl U, Simonis C, Jung S, Kiefer R, Lassmann H, Hartung HP, Haase A, Toyka KV: In vivo MRI, and its histological correlates in acute adoptive transfer experimental allergic encephalomyelitis: quantitation of inflammation and oedema. Brain 1996, 119:239–248
11. Quint DJ, Buckham SP, Bolton EJ, Solari R, Champion BR, Zanders ED: Immunoregulation in the common marmoset, *Callithrix jacchus*: functional properties of T and B lymphocytes and their response to human interleukins 2 and 4. Immunology 1990, 69:616–621
12. Neubert R, Nogueira AC, Neubert D: Thalidomide derivatives and the immune system. 1. Changes in the pattern of integrin receptors and other surface markers on T lymphocyte subpopulations of marmoset blood. Arch Toxicol 1993, 67:1–17
13. Neubert R, Foerster M, Nogueira AC, Helge H: Cross-reactivity of antihuman monoclonal antibodies with cell surface receptors in the common marmoset. Life Sci 1995, 15:317–324
14. Bontrop RE, Otting N, Slierendregt BL, Lanchbury JS: Evolution of major histocompatibility complex polymorphisms and T cell receptor diversity in primates. Immunol Rev 1995, 143:33–62
15. Uccelli A, Oksenberg JR, Jeong M, Genain CP, Rombos T, Jaeger EEM, Giunti D, Lanchbury JS, Hauser SL: Characterization of the TCRB chain repertoire in the New World monkey *Callithrix jacchus*. J Immunol 1997, 158:1201–1207
16. Van Noort JM, El Ouagmir M, Boon J, Van Seghel AC: Fractionation of central nervous system myelin proteins by reversed phase high performance liquid chromatography. J Chromatogr 1994, 653:155–161
17. Bradford MM: A rapid and sensitive method for the quantitation of microgram quantities of protein utilizing the principle of protein-dye binding. Anal Biochem 1976, 72:248–254
18. Massacesi L, Genain CP, Lee-Parritz D, Letvin NL, Canfield D, Hauser SL: Actively and passively induced experimental autoimmune encephalomyelitis in common marmosets: a new model for multiple sclerosis. Ann Neurol 1995, 37:519–530
19. Genain CP, Lee-Parritz D, Nguyen MH, Massacesi L, Joshi N, Ferrante R, Hoffman K, Moseley M, Letvin NL, Hauser SL: In healthy primates, circulating autoreactive T cells mediate autoimmune disease. J Clin Invest 1994, 94:1339–1345
20. Van Lambalgen R, Jonker M: Experimental allergic encephalomyelitis in rhesus monkeys: 1. Immunological parameters in EAE-resistant and susceptible rhesus monkeys. Clin Exp Immunol 1985, 68:100–107
21. Slierendregt BL, Hall M, 't Hart BA, Otting N, Anholts J, Verduyn W, Lanchbury JS, Bontrop RE: Identification of an Mhc-DPB1 allele involved in susceptibility to experimental autoimmune encephalomyelitis in rhesus macaques. Int Immunol 1995, 7:1671–1679
22. Barkhof F, Valk J, Hommes OR, Scheltens P, Nauta JJP: Gadopentetate diglumine enhancement of multiple sclerosis lesions on long TR spin-echo images at 0.6 T. Am J Neuroradiol 1992, 13:1257–1259
23. Laman JD, Van Meurs M, Schellekens MM, De Boer M, Massacesi L, Melchers B, Lassmann H, Claassen E, 't Hart BA: Expression of accessory molecules and cytokines in acute experimental autoimmune encephalomyelitis (EAE) in marmoset monkeys (*Callithrix jacchus*). J Neuroimmunol 1998, 86:30–45
24. Vass K, Lassmann H, Wekerle H, Wisniewski HM: The distribution of Ia-antigen in the lesions of rat acute experimental allergic encephalomyelitis. Acta Neuropathol 1996, 70:149–160
25. Lucchinetti CF, Brück W, Rodriguez M, Lassmann H: Distinct patterns of multiple sclerosis pathology indicates heterogeneity in pathogenesis. Brain Pathol 1996, 6:259–274
26. Piddlesden SJ, Lassmann H, Zimprich F, Morgan BP, Linington C: The demyelinating potential of antibodies to myelin oligodendrocyte

glycoprotein is related to their ability to fix complement. Am J Pathol 1993, 143:555–564
27. Brück W, Porada P, Poser S, Rieckmann P, Hanefeld F, Kretzschmar A, Lassmann H: Monocyte/Macrophage differentiation in early multiple sclerosis lesions. Ann Neurol 1995, 38:788–796
28. Nagara H, Inoue T, Koga T, Kitaguchi T, Tateishi J, Goto I: Formalin-fixed brains are useful for magnetic resonance imaging (MRI) study. J Neurol Sci 1987, 81:67–77
29. Barkhof F, Scheltens PH, Kamphorst W: Pre- and postmortem MR imaging of unsuspected multiple sclerosis in a patient with Alzheimer's disease. J Neurol Sci 1993, 117:175–178
30. Storch MK, Piddlesden S, Haltia M, Iivanainen M, Morgan P, Lassmann H: Multiple sclerosis: in situ evidence for antibody- and complement-mediated demyelination. Ann Neurol 1998, 43:465–471
31. Barkhof F: Imaging of remyelination. Mult Scler 1997, 3:129–132
32. Ozawa K, Suchanek G, Breitschopf H, Brück W, Budka H, Jellinger K, Lassmann H: Patterns of oligodendroglia pathology in multiple sclerosis. Brain 1994, 117:1311–1322